

Aberystwyth University

Age and context of the oldest known hominin fossils from Flores

Brumm, Adam; van den Bergh, Gerrit D.; Storey, Michael; Kurniawan, Iwan; Alloway, Brent V.; Setiwan, Ruly; Setiyabudi, Erick; Grün, Rainer; Moore, Mark W.; Yurnaldi, Dida ; Puspaningrum, Mika R.; Wibowo, Unggul P.; Insani, Halmi; Sutisna, Indra; Westgate, John A.; Pearce, Nicholas; Duval, Mathieu; Meijer, Hanneke J. M.; Aziz, Fachroel; Sutikna, Thomas

Published in:
Nature

DOI:
[10.1038/nature17663](https://doi.org/10.1038/nature17663)

Publication date:
2016

Citation for published version (APA):

Brumm, A., van den Bergh, G. D., Storey, M., Kurniawan, I., Alloway, B. V., Setiwan, R., Setiyabudi, E., Grün, R., Moore, M. W., Yurnaldi, D., Puspaningrum, M. R., Wibowo, U. P., Insani, H., Sutisna, I., Westgate, J. A., Pearce, N., Duval, M., Meijer, H. J. M., Aziz, F., ... Morwood, M. J. (2016). Age and context of the oldest known hominin fossils from Flores. *Nature*, 534, 249-253. <https://doi.org/10.1038/nature17663>

General rights

Copyright and moral rights for the publications made accessible in the Aberystwyth Research Portal (the Institutional Repository) are retained by the authors and/or other copyright owners and it is a condition of accessing publications that users recognise and abide by the legal requirements associated with these rights.

- Users may download and print one copy of any publication from the Aberystwyth Research Portal for the purpose of private study or research.
- You may not further distribute the material or use it for any profit-making activity or commercial gain
- You may freely distribute the URL identifying the publication in the Aberystwyth Research Portal

Take down policy

If you believe that this document breaches copyright please contact us providing details, and we will remove access to the work immediately and investigate your claim.

tel: +44 1970 62 2400
email: is@aber.ac.uk

1 **Stratigraphic context and age of hominin fossils from Middle Pleistocene Flores**

2

3 Adam Brumm^{1,2*}, Gerrit D. van den Bergh^{3*#}, Michael Storey⁴, Iwan Kurniawan^{5*},
4 Brent V. Alloway^{6,3}, Ruly Setiawan^{7,3}, Erick Setiyabudi⁵, Rainer Grün^{8,1}, Mark W.
5 Moore⁹, Dida Yurnaldi^{7,3}, Mika R. Puspaningrum³, Unggul P. Wibowo^{5,3}, Halmi
6 Insani⁵, Indra Sutisna⁵, John A. Westgate¹⁰, Nick J.G. Pearce¹¹, Mathieu Duval¹²,
7 Hanneke J.M. Meijer¹³, Fachroel Aziz⁵, Thomas Sutikna^{3,14}, Sander van der Kaars^{15,16},
8 Michael J. Morwood^{3§}

9

10 **Author affiliations**

11 ¹Research Centre of Human Evolution, Environmental Futures Research Institute,
12 Griffith University, Nathan QLD 4111, Australia.

13 ²School of Earth & Environmental Sciences, University of Wollongong, Wollongong
14 NSW 2522, Australia.

15 ³Centre for Archaeological Science, School of Earth & Environmental Sciences,
16 University of Wollongong, Wollongong NSW 2522, Australia.

17 ⁴Quadlab, Natural History Museum of Denmark, University of Copenhagen, 12 DK-
18 1350 Copenhagen, Denmark.

19 ⁵Geology Museum, Bandung 40122, Indonesia.

20 ⁶School of Geography, Environment and Earth Sciences, Victoria University,
21 Wellington 6012, New Zealand.

22 ⁷Center for Geological Survey, Geological Agency, Bandung 40122, Indonesia.

23 ⁸Research School of Earth Sciences, The Australian National University, Canberra
24 ACT 2601, Australia.

25 ⁹Stone Tools and Cognition International Research Hub, School of Humanities,

26 University of New England, Armidale NSW 2351, Australia.

27 ¹⁰Department of Earth Sciences, University of Toronto, Toronto, Ontario M5S 3B1,
28 Canada.

29 ¹¹Department of Geography & Earth Sciences, Aberystwyth University, Wales SY23
30 3DB, United Kingdom.

31 ¹²Geochronology, Centro Nacional de Investigación sobre la Evolución Humana
32 (CENIEH), Paseo de Atapuerca, 3, 09002-Burgos, Spain.

33 ¹³University Museum of Bergen, University of Bergen, 5007 Bergen, Norway.

34 ¹⁴National Research Centre for Archaeology (ARKENAS), Jakarta 12510, Indonesia.

35 ¹⁵Cluster Earth & Climate, Faculty of Earth and Life Sciences, Vrije Universiteit, HV
36 1081 HV Amsterdam, the Netherlands.

37 ¹⁶School of Earth, Atmosphere and Environment, Monash University, Clayton VIC
38 3800, Australia.

39 [§]Deceased

40 **These authors contributed equally*

41

42 [#]Correspondence and requests for information should be addressed to G.D.v.d.B.

43 (gert@uow.edu.au)

44

45 **Recent excavations at the early Middle Pleistocene site of Mata Menge in the So'a**
46 **Basin of central Flores, Indonesia, have yielded fossils of hominins¹ attributed to**
47 **a population ancestral to Late Pleistocene *Homo floresiensis*². Here we describe**
48 **the context and age of the Mata Menge hominin specimens and associated**
49 **archaeological findings. The fluvial sandstone layer from which the *in situ* fossils**
50 **were excavated in 2014 was deposited in a small valley stream around 700**

51 thousand years (kyr) ago, as indicated by $^{40}\text{Ar}/^{39}\text{Ar}$ and fission track dates on
52 stratigraphically bracketing volcanic ash and pyroclastic density current
53 deposits, in combination with coupled Uranium-series (U-series) and Electron
54 Spin Resonance (ESR) dating of fossil teeth. Palaeoenvironmental data indicates
55 a relatively hot and dry climate in the So'a Basin during the early Middle
56 Pleistocene, while various lines of evidence suggest the hominins inhabited a
57 savannah-like open grassland habitat with a strong wetland component. The
58 hominin fossils occur alongside the remains of an insular fauna and a simple,
59 'Mode 1'-like stone technology that is markedly similar to that of *H. floresiensis*.

60

61 Mata Menge is located near the northwestern margin of the So'a Basin, a $\sim 400 \text{ km}^2$
62 geological depression in the interior highlands of central Flores (Fig. 1). The basement
63 substrate consists of the Ola Kile Formation (OKF), a $>100 \text{ m}$ -thick sequence of
64 indurated volcanoclastic deposits dominated by andesitic breccia and locally
65 alternating with lava flows, tuffaceous sandstones, and siltstones^{3,4}. Zircon fission-
66 track (ZFT) age determinations date the upper part of the OKF to 1.86 ± 0.12 million
67 years ago (Ma) (ref. 4). The OKF is unconformably overlaid by the Ola Bula
68 Formation (OBF)^{3,4}. The latter is up to 120 m thick, and comprises an intra-basinal
69 fossil- and stone artefact-bearing sequence deposited between 1.8 to 0.5 Ma . The $\sim 5^\circ$
70 southward dipping volcanic breccias of the OKF are associated with a former volcanic
71 centre located on the northwestern edge of the basin. Inside the remnant of this 10 km
72 diameter caldera structure, known as the Welas Caldera, are well-formed intra-caldera
73 lake sediments punctuated by two intra-caldera basaltic cones that were the major
74 sources of primary and secondary basaltic volcanoclastic deposits within the OBF.

75

76 Since the 1950s, palaeontological and archaeological research in the So'a Basin has
77 focused on the OBF⁵⁻¹⁴, which is composed largely of undistorted volcanic, fluvial,
78 and lacustrine sediments^{3,4}. The volcanoclastic aprons that entered the central
79 depression from various directions, at times debouching into a lake, or series of small
80 lakes, were incised by erosional gullies during periods of volcanic quiescence, but
81 became sites of enhanced accretion following major volcanic influxes. Well-developed
82 paleosols and pedogenically altered fine-grained fluvial deposits intervening
83 between variably textured pyroclastic (primary) and fluvio-volcanoclastic (secondary)
84 deposits document intermittent periods of landscape stability that alternated with rapid
85 depositional events triggered by major volcanic eruptions, generating airfall tephra,
86 ignimbrites, and associated mass-flow deposits (see SI Table 1). A basin-wide, thinly-
87 bedded lacustrine sequence, consisting of an alternation of thin-bedded micritic
88 freshwater limestones, clays, and with numerous basaltic tephra inter-beds – the 'Gero
89 Limestone Member' (GLM) – caps the basin infill and registers the formation of a
90 basin-wide lake^{3,4}, which formerly extended into the Welas Caldera.

91
92 The total preserved thickness of the OBF at Mata Menge, up to the top of an adjacent
93 hill northwest of the site, is 40 m (Fig. 1). The uppermost interval of the GLM, with a
94 thickness of 9 m, outcrops at the summit of a hill 600 m west (Excavation #35, or E-
95 35). The main fossil-bearing intervals at Mata Menge form part of a roughly NNW-
96 SSE trending palaeovalley dominantly occupied by a sequence of cut-and-fill
97 fluvial and clay-rich mass-flow deposits. The hominin-bearing sedimentary layer
98 lies at the head of a modern dry stream valley at the base of a hill (ht = 397m). A slot-
99 trench excavated into the eastern side of this hill revealed an 18 m-thick sequence of
100 planar bedded lacustrine clays and micritic limestones containing oogonia and

101 diatoms, fluvial sandstone beds, massive tuffaceous clay-rich mass-flow (mudflow)
102 deposits, fine-grained well-developed clay-textured paleosols, and numerous
103 centimetre-thick basaltic tephra inter-beds, pertaining to the middle upper part of the
104 OBF. At the base of this slot-trench, a thin (<30 cm-thick) fossil-bearing fluvial
105 sandstone layer was exposed underlying a sequence of mudflow deposits (Layers Ia-f)
106 up to 6.5 m thick. This fossiliferous sandstone, named Layer II, represents the deposit
107 of a small stream channel that has an irregular lower bedding plane and was incised
108 into a well-developed, consolidated paleosol with prominent root traces (Layer III).
109
110 We conducted a 50 m² excavation (E-32) into Layer II in 2013 (Fig. 1 and Extended
111 Data Figs. 1-2). The sandstone layer yielded fossils of the dwarfed proboscidean
112 *Stegodon florensis*⁸, and numerous well-preserved dental and skeletal remains of giant
113 rat (*Hooijeromys nusatenggara*)¹⁵, as well as teeth of Komodo dragon (*Varanus*
114 *komodoensis*) and crocodiles, and flaked stone artefacts (Fig. 2). In 2014, we exposed
115 Layer II over a larger area by extending the initial trench (E-32A) to the south (E-
116 32B/C) and west (E-32D/E). A separate excavation was also opened upstream of the
117 palaeo-channel to the north (E-32F). These excavations recovered six hominin teeth
118 and a hominin mandible fragment from Layer II (ref. 1). Another less diagnostic
119 hominin fossil comprises a 60 mm² piece of a cranial vault. The hominin fossils
120 occurred at the stratigraphic interface between Layer II and the overlying mudflow
121 deposit, spread over a maximum linear distance of 15 m. The flow direction in the
122 sinuous stream tributary in which Layer II was deposited was from NNW to SSE,
123 based on the slight decrease in elevation of the top of this layer in the same direction
124 (i.e., 20 cm over a horizontal distance of 17 m). The fine- to medium-grained fluvial
125 sandstone has a maximum thickness of 30 cm, contains scattered pebbles, and occurs

126 13 m stratigraphically above the main (lower) fossil-bearing beds at Mata Menge,
127 which have a combined thickness of up to two metres (Fig. 1).
128

129 The mudflow sequence (Layers Ia-f) sealing in Layer II can be clearly related to
130 phreatomagmatic to magmatic eruptive activity occurring within the confines of the
131 Welas Caldera (then occupied by a lake). The formation of these multiple mudflow
132 events either relates to intermittent displacement of lake waters down adjacent
133 tributaries during cone construction, or, alternatively, failure of a lake outlet barrier
134 during and/or following intra-caldera eruptive activity. Four articulated thoracic
135 vertebrae of *S. florensis* were recovered from Layer II (Fig. 2k) near a concentration
136 of other vertebrae, ribs, and postcranial remains of a *Stegodon* carcass. These are the
137 only articulated stegodont elements so far recovered at Mata Menge, indicating
138 relatively limited post-mortem modification prior to burial by mudflows. We infer
139 that the artefacts and faunal remains, including the hominin elements, were exposed
140 to weathering on the ground surface, and could have been transported short distances
141 by the small stream, before a series of mudflows originating from the intra-caldera
142 lake system were channelized within adjacent stream tributaries, inundating these
143 valleys with metre-thick muddy debris. It is conceivable that the presence of elements
144 from multiple hominin individuals, including two juveniles, and several individual
145 stegodonts, could be the result of a volcanic event. However, other explanations are
146 also possible and more research into taphonomic factors is needed.
147

148 A total of four new radiometric determinations, with ages in sequential order and in
149 accordance with the stratigraphic sequence, as well as previously published estimates,
150 provide a robust chronological framework for the hominin fossils (Fig. 1; see also

Supplementary Information). Near the base of the OBF at Mata Menge, a widespread ignimbritic marker bed (the Wolo Sege Ignimbrite; T-WSI) with an $^{40}\text{Ar}/^{39}\text{Ar}$ age of 1.01 ± 0.02 Ma (ref. 13; and see Fig. 1) is recognised on the combined basis of its stratigraphic association, unique depositional architecture, and glass-shard major element chemistry (see Extended Data Fig. 3). In addition, the hominin find-locality in E-32 is situated 12.5 m stratigraphically above a ZFT date of 0.80 ± 0.07 Ma from Mata Menge⁴. To verify this prior estimate⁴, we conducted Isothermal Plateau Fission-Track (ITPFT) dating of glass shards from an inter-regional tephra marker (T3) identified at several So'a Basin localities, including just above the T-WSI at Mata Menge (in E-34/34B), returning a weighted mean age of 0.90 ± 0.07 Ma (based on two independent age determinations) (see Extended Data Fig. 3). Moreover, $^{40}\text{Ar}/^{39}\text{Ar}$ single crystal dating of hornblende from the Pu Maso Ignimbrite (T-Pu) located just above T3 in E-34/34B yielded a weighted mean age of 0.81 ± 0.04 Ma, which is stratigraphically consistent with that of underlying T3 (Extended Data Fig. 4). These ages demonstrate that Layer II was deposited after ~ 0.80 Ma.

To further constrain the age of the hominin fossils, we carried out $^{40}\text{Ar}/^{39}\text{Ar}$ dating on one basaltic tephra and one rhyolitic tephra from the GLM above Layer II (E-12 and E-35). The GLM contains at least 85 crystal-rich tephra inter-beds of basaltic composition, collectively named the Piga Tephra (the lower 56 tephra are sequentially numbered PGT-1 to PGT-56). At Mata Menge, PGT-2 occurs 13.5 m above Layer II, and produced a $^{40}\text{Ar}/^{39}\text{Ar}$ weighted mean age of 0.65 ± 0.02 Ma from single crystal dating of hornblende (Extended Data Fig. 5). This is in accordance with the published ZFT age of a basaltic tephra inter-bed from the lower part of the GLM (0.65 ± 0.06 Ma)⁴. Finally, a biotite-bearing vitric-rich ash of distinctive rhyolitic

176 composition (T6; see Extended Data Fig. 3) from the top of the GLM has an $^{40}\text{Ar}/^{39}\text{Ar}$
177 age of 0.51 ± 0.03 Ma, based on the weighted mean of single grain feldspar analyses.
178 Thus, the hominin fossils constrained by the lowermost of these two radiometric dates
179 within the GLM have an established minimum age of ~ 0.65 Ma.

180

181 In order to demonstrate that the hominin fossils and associated faunal assemblage do
182 not reflect vertical displacement of chronologically more recent finds into older
183 sediments, we conducted laser ablation U-series analysis of a hominin tooth root
184 fragment from Layer II (specimen SOA-MM6), and combined U-series/ESR-dating
185 of two *S. florensis* molars excavated *in situ* from the same sedimentary context (see
186 Extended Data Fig. 7 and Supplementary Information). U-series dating of the hominin
187 tooth root independently confirms this specimen was deposited at least 0.55 Ma,
188 whereas combined U-series/ESR indicates minimum and maximum ages of around
189 0.36 Ma and 0.69 Ma, respectively, for the *Stegodon* molars. In sum, therefore, we
190 have used multiple dating methods to establish a secure age of ~ 0.70 Ma for the Layer
191 II hominin fossils.

192

193 Our systematic, high-volume excavations (~ 560 m²) at Mata Menge between 2010–15
194 have yielded a wealth of fossil vertebrate remains (see Supplementary Information).
195 To date, 75% of the >7000 vertebrate fossils recovered from E-32 have been
196 analyzed, and include *S. florensis* (23.7% of the number of identified specimens, or
197 NISP), *V. komodoensis* (0.6% of NISP), freshwater crocodiles (3.7% of NISP), frogs
198 (0.3% of NISP), murine rodents (15.6 % of NISP), and birds (0.5% of NISP), the
199 remainder comprising unidentifiable bone fragments. From the lower fossil-bearing
200 interval (E-1 to 8 and E-11 to 31D) the remains of least 120 *S. florensis* individuals

201 are represented by dental elements spanning all ontogenetic stages¹⁶. The age profile
202 of the Mata Menge lower level death assemblage corresponds to that of a living
203 population, suggesting a mass death event. The lack of age-selective mortality does
204 not fit a pattern of hominin predation, such as in the *H. floresiensis* type-locality,
205 Liang Bua¹⁷. In Layer II, remains of juvenile, sub-adult, intermediate-aged, and very
206 old *Stegodon* individuals are also present, but the Minimum Number of Individuals is
207 too low to allow for the construction of a reliable age profile.

208

209 We conducted carbon and oxygen isotope analysis of tooth enamel samples collected
210 from several *S. florensis* and murine rodent individuals from the two fossil-bearing
211 levels at Mata Menge (Extended Data Fig. 8). The results indicate a diet heavily
212 dominated by C₄ grasses, suggesting both animals were grazers, and implying that
213 open grasslands were the major vegetation type in the So'a Basin. The recovery of
214 rare fossils of rails, swans, ducks, eagles, and eagle owls from the lower trenches
215 (~0.80 to 0.88 Ma) further evidences the presence of a savannah-like biome with a
216 strong wetland component, as well as scattered patches of forest¹⁸. Fossil pollen and
217 phytoliths from both fossil levels, while poorly preserved, offer additional evidence
218 that grasses dominated the Middle Pleistocene vegetation (SI Table 9). Abundant
219 moulds and casts of two species of freshwater gastropods (Cerithioidea) were
220 recovered from Layer II and the base of the overlying mudflow sequence, pointing to
221 the existence of permanent freshwater bodies in the ancestral stream valley.

222

223 Our excavations uncovered 149 *in situ* stone artefacts in E-32, including 47 artefacts
224 from Layer II, in direct association with the hominin remains (Fig 2; Extended Data
225 Fig. 9). Some of the artefacts from E-32 are lightly to heavily abraded from low-

energy water transport¹⁹, but 74.5% are in fresh, as-struck condition, suggesting minimal dislocation from nearby stone-flaking areas. Hominins gathered coarse- to fine-grained rounded volcanic cobbles from local fluvial gravels and struck them with hammerstones to create sharp-edged flakes and cores. Reduction was mostly bifacial, with blows struck to two faces of the stone from one platform edge (Fig 2a). Two cores were rotated and a second bifacial platform edge was established, resulting in multi-platform cores. Core platform surfaces or edge-angles were unprepared, and core reduction was not intensive. The edges of flakes struck from these cores were sometimes retouched for use, or possibly to produce additional flake tools. One heavily abraded core was scavenged and further flaked. Overall, the E-32 assemblage reflects a technologically straightforward core-and-flake approach to stoneworking²⁰. The function of the implements is unknown; as yet, no butchery marks have been conclusively identified on the faunal remains at Mata Menge, and the tools may have been used for modifying other organic materials.

240

Notably, the tools and flaking technology in E-32 are nearly identical in size and nature, respectively, to the assemblage dating some 110 kyr earlier at Mata Menge^{12,21-23}, including 1186 analysed stone artefacts from E-23 and E-27 excavated between 2011–14 (Table S6). The E-32 assemblage is also technologically similar to the artefacts from Liang Bua, dating ~600 kyr later^{12,24} and associated with *H. floresiensis*^{25,26}. The long persistence of this technical approach to stone-flaking on Flores¹², together with the close anatomical similarities between the Mata Menge and Liang Bua hominins¹, suggests remarkable stability in the behaviour of the *H. floresiensis* lineage. In contrast, the only lithic assemblage thus far recovered *in situ* below the T-WSI, which has a minimum age of 1.01 ± 0.02 Ma and is therefore the

earliest known stone technology from Flores¹³, whilst also ‘Mode 1’ in character,
features a typologically distinct element: large Acheulean pick-like implements²⁷ that
in Lower Palaeolithic industries of Africa and western Eurasia are emblematic of
cognitively advanced tool-making^{20,28-29}. The reason for the absence of these more
sophisticated components from the later technology of Flores remains unknown;
however, possible explanations include: i) a reduction in the behavioural flexibility of
Homo erectus due to island-dwarfing¹; ii) by ~880 Ma the hominin population size
had dropped below a minimum threshold required to maintain cultural complexity³⁰;
iii) the older, Acheulean-like artefacts were made by a separate hominin lineage.

260

261 **References**

262

263 1. van den Bergh, G. D. *et al.* *Homo floresiensis*-like hominin fossils from the Middle
264 Pleistocene of Flores. *Nature* (submitted).

265

266 2. Brown, P. *et al.* A new small-bodied hominin from the Late Pleistocene of Flores,
267 Indonesia. *Nature* **431**, 1055–1061 (2004).

268

269 3. Morwood, M. J. O’Sullivan, P. B., Aziz, F. & Raza, A. Fission-track ages of stone
270 tools and fossils on the east Indonesian island of Flores. *Nature* **392**, 173–176 (1998).

271

272 4. O’Sullivan, P. B. *et al.* Archaeological implications of the geology and chronology
273 of the Soa Basin, Flores, Indonesia. *Geology* **29**, 607–610 (2001).

274

275 5. Maringer, J. & Verhoeven, Th. Die Steinartefakte aus der *Stegodon*-Fossilschicht

- 276 von Mengeruda auf Flores, Indonesien. *Anthropos* **65**, 229–247 (1970).
277
- 278 6. Maringer, J. & Verhoeven, Th. Die Oberflächenfunde aus dem Fossilgebiet von
279 Mengeruda und Olabula auf Flores, Indonesien. *Anthropos* **65**, 530–546 (1970).
280
- 281 7. Sondaar, P. Y. *et al.* Middle Pleistocene faunal turn-over and colonisation of Flores
282 (Indonesia) by *Homo erectus*. *C.R. Acad. Sci.* **319**, 1255–1262 (1994).
283
- 284 8. Morwood, M. J. *et al.* Stone artefacts from the 1994 excavation at Mata Menge,
285 West Central Flores, Indonesia. *Aust. Archaeol.* **44**, 26–34 (1997).
286
- 287 9. van den Bergh, G. D. *The Late Neogene Elephantoid-Bearing Faunas of Indonesia*
288 *and their Palaeozoogeographic Implications. A Study of the Terrestrial Faunal*
289 *Succession of Sulawesi, Flores and Java, including Evidence for Early Hominid*
290 *Dispersal East of Wallace's Line* (Scripta Geologica 117, Nationaal Natuurhistorisch
291 Museum, 1997).
292
- 293 10. van den Bergh, G. D. *et al.* Did *Homo erectus* reach the island of Flores? *Bull.*
294 *Indo. Pac. Pre. Hi.* **14**, 27–36 (1996).
295
- 296 11. Morwood, M. J. *et al.* Archaeological and palaeontological research in central
297 Flores, east Indonesia: results of fieldwork 1997-98. *Antiquity* **73**, 273–286 (1999).
298
- 299 12. Aziz, F. & Morwood, M. J., in *Pleistocene Geology, Palaeontology and*
300 *Archaeology of the Soa Basin, Central Flores, Indonesia* (eds Aziz, F., Morwood, M.

301 J. & van den Bergh, G. D.) 1–18 (Spec. Publ. 36, Geological Survey Institute, 2009).
302
303 13. Brumm, A. *et al.* Early stone technology on Flores and its implications for *Homo*
304 *floresiensis*. *Nature* **441**, 624–628 (2006).
305
306 14. Brumm, A. *et al.* Hominins on Flores, Indonesia, by one million years ago. *Nature*
307 **464**, 748–753 (2010).
308
309 15. Musser, G. G. The giant rat of Flores and its relatives east of Borneo and Bali. *B.*
310 *Am. Mus. Nat. Hist.* **169**, 67–176 (1981).
311
312 16. van den Bergh, G. D. *et al.* Taphonomy of *Stegodon florensis* remains from the
313 early Middle Pleistocene archaeological site Mata Menge, Flores, Indonesia. Abstract
314 book of the VIth International Conference on Mammoths and their relatives. *S.A.S.G.*,
315 *Special Volume* **102**, 207–208 (2014).
316
317 17. van den Bergh, G. D. *et al.* The Liang Bua faunal remains: a 95 k.y.r. sequence
318 from Flores, East Indonesia. *J. Hum. Evol.* **57**, 527–537 (2009).
319
320 18. Meijer, H. J. M. *et al.* Avian remains from the Early/Middle Pleistocene of the
321 So’a Basin, central Flores, Indonesia, and their palaeoenvironmental significance.
322 *Palaeogeogr. Palaeocl.* **440**, 161–171 (2015).
323
324 19. Shea, J. J. Artifact abrasion, fluvial processes, and “living floors” from the Early
325 Paleolithic site of ‘Ubeidiya (Jordan Valley, Israel). *Geoarchaeology* **14**, 191–207

326 (1999).

327

328 20. Moore, M. W. The design space of stone flaking: implications for cognitive
329 evolution. *World Archaeol.* **43**, 702–715 (2011).

330

331 21. Brumm, A. *et al.* Stone technology at the Middle Pleistocene site of Mata Menge,
332 Flores, Indonesia. *J. Arch. Sci.* **37**, 451–473 (2010).

333

334 22. Moore, M. W. & Brumm, A. Stone artifacts and hominins in island Southeast
335 Asia: new insights from Flores, eastern Indonesia. *J. Hum. Evol.* **52**, 85–102 (2007).

336

337 23. Moore, M. W. & Brumm, A. in *Interdisciplinary Approaches to the Oldowan* (eds
338 Hovers, E. & Braun, D. R.) 61–69 (Springer, 2009).

339

340 24. Moore, M.W. *et al.* 2009. Continuities in stone flaking technology at Liang Bua,
341 Flores, Indonesia. *J. Hum. Evol.* **57**, 503–526 (2009).

342

343 25. Morwood, M. J. *et al.* Archaeology and age of a new hominin from Flores in
344 eastern Indonesia. *Nature* **431**, 1087–1091 (2004).

345

346 26. Sutikna, T. *et al.* Revised stratigraphy and chronology for *Homo floresiensis* at
347 Liang Bua, eastern Indonesia. *Nature* (under review).

348

349 27. Brumm, A. & Moore, M. W. Biface distributions and the Movius Line: a
350 Southeast Asian perspective. *Aust. Archaeol.* **74**, 32–46 (2012).

351

352 28. Beyene, Y. *et al.* The characteristics and chronology of the earliest Acheulean at
353 Konso, Ethiopia. *Proc. Natl Acad. Sci. USA* **110**, 1584–1591 (2013).

354

355 29. Wynn, T. Archaeology and cognitive evolution. *Behav. Brain Sci.* **25**, 389–402
356 (2002).

357

358 30. Powell, A. *et al.* Late Pleistocene demography and the appearance of modern
359 human behavior. *Science* **324**, 1298–1301 (2009).

360

361

362 **Supplementary Information** is available in the online version of the paper.

363

364 **Acknowledgments**

365 The So'a Basin project was funded by an Australian Research Council (ARC)
366 *Discovery* grant (DP1093342) awarded to M.J.M. and A.B., and directed by M.J.M.
367 (2010-2013) and G.v.d.B. (2013-2015), while the Geological Survey Institute (GSI)
368 of Bandung, Indonesia, provided financial and technical support. G.v.d.B.'s research
369 was also supported by ARC Future Fellowship FT100100384. Quadlab is funded by a
370 grant to M.S. from the Villum Foundation. M.D. received funding from a Marie Curie
371 International Outgoing Fellowship of the EU's Seventh Framework Programme
372 (FP7/2007-2013), awarded under REA Grant Agreement No. PIOF-GA-2013-
373 626474. For permission to undertake this research, we thank the Indonesian State
374 Ministry of Research and Technology (RISTEK), the former Heads of the Geological
375 Agency (R. Sukyiar and Surono), the successive directors of the GSI (S.

376 Permanandewi, Y. Kusumahbrata [formerly] and A. Pribadi) and Bandung's Geology
377 Museum (S. Baskoro and O. Abdurahman). Local research permissions were issued
378 by the provincial government of East Nusatenggara at Kupang, and the Ngada and
379 Nage Keo administrations. We also thank the Ngada Tourism and Culture and
380 Education Departments for their ongoing support. In addition, we acknowledge
381 support and advice provided by I. Setiadi, D. Pribadi and Suyono (GSI), the National
382 Centre for Archaeology (ARKENAS) in Jakarta, and J.T. Solo of the provincial
383 Culture and Tourism office in Kupang. Scientific and technical personnel involved in
384 the fieldwork included: T. Suryana, S. Sonjaya, H. Oktariana, I. Sutisna, A. Rahman,
385 S. Bronto, E. Sukandar, A. Gunawan, Widji, A.S. Hascaryo, Jatmiko, S. Wasisto,
386 R.A. Due, S. Hayes, Y. Perston, B. Pillans, K. Grant, M. Marsh, D. McGahan, A.M.
387 Saiful, Basran, M. Tocheri, A. R. Chivas and S. Flude. Sidarto (GSI) provided DEM
388 data used in Fig. 1b. Geodetic surveys and measurements were conducted by E.E.
389 Laksmana, A. Rahmadi and Y. Sofyan. J. Noblett constructed the Mata Menge 3D
390 model, based on drone aerial photographs taken by K. Riza, T.P. Ertanto, and M.
391 Faizal. The research team was supported by ~100 excavators and support personnel
392 from the Ngada and Nage Keo districts. R.G. and M.D. thank L. Kinsley, RSES, The
393 Australian National University, for his assistance with the mass spectrometric
394 measurements.

395

396

397 **Author contributions**

398 A.B., G.D.v.d.B., I.K. and M.J.M. directed the Mata Menge excavations. M.S., B.A.
399 and R.S. collected tephra samples and M.S. undertook $^{40}\text{Ar}/^{39}\text{Ar}$ dating.
400 G.D.v.d.B. described the site stratigraphy, with R.S., D.Y. and B.V.A.. J.A.W.

401 conducted ITPFT-dating of T3 with B.V.A. and comparative trace element analyses
402 of interregional markers (with N.J.P. & B.V.A.). E.S., F.A. and T.S. oversaw key
403 aspects of the field project. M.W.M. analysed the stone assemblage, and G.D.v.d.B.,
404 H.I., I.S., M.R.P. U.P.W. and H.J.M.M. analysed the fauna. M.P. conducted isotopic
405 analyses, R.G. and M.D. undertook U/Th and ESR analyses of faunal remains, and
406 S.v.d.K. carried out the palynological analysis. A.B. and G.D.v.d.B. prepared the
407 manuscript, with contributions from other authors.

408

409 **Figure legends (main text)**

410

411 **Figure 1:** Context and chronology of the hominin fossils at Mata Menge. **a-b**,
412 location of Flores and the So'a Basin; **c**, Digital Elevation Map of the So'a Basin,
413 showing the location of Mata Menge and other sites mentioned in the text. A single
414 outlet of the main river system (the Ae Sissa) drains the basin via a steep-walled
415 valley towards the northeast; **d**, stratigraphy and chronology of the main fossil-
416 bearing intervals and intervening Ola Bula Formation (OBF) deposits at Mata Menge.
417 Several basin-wide key marker tephra beds that are exposed in the hill flank on the
418 northern side of Mata Menge (trench E-34/34B) are eroded in the central part of the
419 stream valley, where they are replaced by a 4-5 m thick sequence of tuffaceous
420 mudflows with intervening fluvial lenses forming the lower fossil-bearing
421 paleovalley-fill sequence; **e-f**, context of the hominin fossils; **f** is a 3D image of Mata
422 Menge and surrounds, with excavated trenches outlined in red and labelled, and **e** is a
423 3D representation of the stratigraphy exposed by trench E-32A-E, with coloured ovals
424 denoting the positions of *in situ* hominin fossils (SOA-MM1, 2 and 4-6) excavated
425 from the fluvial sandstone unit, Layer II. Trenches E-1 to E-8 were excavated

between 2004-06, at the section originally excavated by Th. Verhoeven in the
 1950s^{5,6}. The remaining trenches were excavated between 2010 to 2015. Tephra codes
 in **d** are as follows (top to bottom): T6 (upper inter-regional tephra); PGT-2 (Piga
 Tephra 2); T-UMM (Upper Mata Menge Tephra); T-LMM (Lower Mata Menge
 Tephra); T-Pu (Pu Maso Tephra); T3 (lower inter-regional tephra); T-T (Turakeo
 Tephra); T-WSI (Wolo Sege Ignimbrite); T-W (Wolowawu Tephra). The original
 published ⁴⁰Ar/³⁹Ar age for T-WSI is 1.02 ± 0.02 Ma (ref. 13); however, when
 recalculated to the recently determined value for the age standard ACS-2 used in this
 study (1.185 Ma; see SI ref. 25), T-WSI becomes 1.01 ± 0.02 Ma.

Figure 2: Stone artefacts and fossils from Mata Menge. All specimens are from the
 hominin fossil find-locality (Layer II fluviatile sandstone, Trench E-32). **a**, bifacial
 core (chlorite); **b-c**, chert flakes; **d**, chalcedony flake; **e**, rhyolite flake; **f**, right maxilla
 fragment (M1-M3), *Hooijeromys nusatenggara*; **g**, left mandible fragment (m1-m3, i)
H. nusatenggara; **h**, right maxilla fragment, *Varanus komodoensis*; **i**, crocodile tooth;
j, right coracoid of a duck (cf. *Tadorna*); **k**, *Stegodon florensis* thoracic vertebrae in
 articulation (still partially embedded in sandstone matrix). Scale bar lengths: **a-i** = 10
 mm; **j** = 100 mm.

Figure legends (extended data)

Extended Data Figure 1. Hominin fossil find-locality at Mata Menge. **a**, View of
 Excavation 32 (trench E-32) in 2014, taken towards the north-north-west. The dip
 slope visible in the background is the eastern flank of the Welas Caldera, which was

451 the source for many of the volcanic products deposited in the So'a Basin; **b**, E-32A-E
452 viewed towards the southwest, in October 2015; **c**, E-32D to E-32E viewed towards
453 the southwest. The irregular erosional upper surface of the reddish brown paleosol
454 (Layer III) formed the hardened bedding of a small stream. The sandy fossil-bearing
455 Layer II infills depressions formed on this bedding surface. A sequence of mudflows
456 (Layer I/a-f) rapidly covered the entire river bedding and its exposed banks; **d**, Mold
457 of a freshwater gastropod (Cerithoidea) from a sandy lens in Layer II; **e**, Detail of the
458 locally developed, gradual boundary between sandy Layers II and muddy Layer I.
459 Note the abundance of muddy rip clasts around the transition. At other places, the
460 boundary is sharp; **f**, West baulk of E-32C. Large *Stegodon florensis* bones occur at
461 the boundary between Layers II and I.

462

463 **Extended Data Figure 2: Plan and baulk profiles of Excavation 32A-F showing**
464 **distribution of finds.** The horizontal plan (lower left corner) shows the horizontal
465 coordinates of individual fossil finds (green crosses) and stone artefacts (blue
466 diamonds). The original position of hominin fossils is indicated with red stars. In the
467 trench baulk profiles (top and right) only the projected positions of fossil finds
468 occurring within one meter of the baulks are plotted. All hominin fossils were
469 recovered from the top of sandy Layer II. The basal part of the mudflow unit (Layers
470 Ia-e) also contains fossils, stone artefacts, gastropods, and pebbles. The thick brown
471 dotted line indicates the western margin of the ancient streambed.

472

473 **Extended Data Figure 3: ITPFT dating and glass chemistry analysis. a-c,**
474 Selected major element compositions (weight percent FeO vs. K₂O and CaO and SiO₂
475 vs. K₂O) of glass shards from key rhyolitic pyroclastic density current (PDC) and

476 airfall deposits at Mata Menge; **d-h**, Weight percent FeO versus CaO composition of
477 glass shards from key rhyolitic pyroclastic density current (PDC) and airfall deposits
478 at Mata Menge (in stratigraphic sequence – youngest to oldest) compared with
479 correlatives from adjacent So'a Basin sites. While the major element glass
480 compositions of T-WSI, T-T and T-Pu are all geochemically indistinguishable (i.e.,
481 they are most likely from the same eruptive source) the major element data for each of
482 the tephra consistently occupies different overlapping fields. Moreover, while subtle
483 geochemical differences exist between T-WSI, T-T and T-Pu, these tephra can also be
484 readily distinguished in the field by a combination of stratigraphic position and
485 association, as well as by morphological expression; **i-j**, Selected trace element
486 compositions Sr versus Th and Zr, and **(k-m)** Y versus Nb, Ce and Th of glass shards
487 from T3 correlatives at Mata Menge, Lowo Mali and Kopowatu as well as T6
488 (uppermost inter-regional marker) from Mata Menge. All trace element
489 concentrations are in ppm unless otherwise stated. This data is plotted against
490 equivalent elemental mean and standard deviation (represented as $\pm 1\sigma$ error bars)
491 reference data from potential distal tephra correlatives (i.e. Youngest Toba Tuff
492 [YTT], Middle Toba Tuff [MTT], Oldest Toba Tuff [OTT] and Unit E from ODP-
493 758) acquired on the same instrument using the same standards and under the same
494 analytical conditions^{31,32}. Trace element data indicates that the upper (T6) and lower
495 (T3) inter-regional marker beds occurring at Mata Menge cannot be geochemically
496 related to any known Toba-sourced tephra. On this basis, the eruptive sources of T6
497 and T3 currently remain unknown. However, this absence of eruptive source certainly
498 does not diminish their importance within the overall So'a Basin stratigraphy.

499

500 **Extended Data Figure 4: $^{40}\text{Ar}/^{39}\text{Ar}$ dating results. a**, Age probability plot for single

crystal laser fusion data for hornblende from the Pu Maso ignimbrite (sample FLO-15-15; SI Table 5); the vertical scale is a relative probability measure of a given age occurring in the sample³³. We applied an outlier-rejection scheme to the main population to discard ages with normalized median absolute deviations of >1.5 (ref. 34) and these are shown as open circles. % $^{40}\text{Ar}^*$ refers to the proportion of radiogenic ^{40}Ar released for individual analyses. The weighted mean age of the filtered hornblende data for the Pu Maso ignimbrite is 0.81 ± 0.04 Ma (1σ ; $\text{mswd} = 0.59$, $\text{prob} = 0.93$; $n = 23/29$). An inverse isochron plot (**b**) for these 23 analyses gives a statistically overlapping age of 0.78 ± 0.07 Ma (1σ ; $\text{mswd} = 0.6$, $\text{prob.} = 0.92$). The $^{40}\text{Ar}/^{36}\text{Ar}$ intercept of 303 ± 10 is statistically indistinguishable from the atmospheric ratio of 298.6 ± 0.3 (ref. 35), thus supporting the more precise weighted mean age result.

Extended Data Figure 5: $^{40}\text{Ar}/^{39}\text{Ar}$ dating results. **a**, Age probability plot for single crystal laser fusion data for hornblende from the PGT-2 tephra (sample T XII 252-261; SI Table 5). $^{40}\text{Ar}^*$ ranges from $< 10\%$ to nearly 60% . The weighted mean age of the filtered hornblende data for the PGT-2 tephra is 0.65 ± 0.02 Ma (1σ ; $\text{mswd} = 0.78$, $\text{prob} = 0.71$; $n = 17/24$). An inverse isochron plot (**b**) gives a statistically overlapping, but less precise age of 0.61 ± 0.04 Ma (1σ ; $\text{mswd} = 1$, $\text{prob.} = 0.19$).

Extended Data Figure 6: $^{40}\text{Ar}/^{39}\text{Ar}$ dating results. **a**, Age probability plot for single crystal laser fusion data for anorthoclase from the T6 upper inter-regional rhyolitic tephra (sample FLO15-09/2; SI Table 5). $^{40}\text{Ar}^*$ ranges from 20% to nearly 100% . The weighted mean age of the filtered feldspar data for the T6 tephra is 0.51 ± 0.03 Ma (1σ ; $\text{mswd} = 0.20$, $\text{prob} = 0.94$; $n = 5/8$). An inverse isochron plot (**b**) gives a

526 statistically overlapping, but less precise age of 0.45 ± 0.04 Ma (1σ ; $\text{mswd} = 0.8$,
527 $\text{prob.} = 0.54$).

528

529 **Extended Data Figure 7: U-series and ESR samples and dating results. a,**
530 Hominin tooth root samples (#3543A and #3543B) from Layer II, Mata Menge; **b, d,**
531 U-series laser tracks for *Stegodon* molar samples from Layer II; **e, f,** Dose response
532 curves obtained for the two powder enamel samples from #3541 and #3544,
533 respectively. Fitting was carried out with a SSE function through the pooled mean
534 ESR intensities derived from each repeated measurement. Given the magnitude of the
535 D_E values, the correct D_E value was obtained for $5 > D_{\text{max}}/D_E > 10$ (ref. 36).

536

537 **Extended Data Figure 8. Carbon and oxygen isotope analysis of dental enamel. a,**
538 $\delta^{13}\text{C}$ and $\delta^{18}\text{O}$ values of *Stegodon florensis* and murine rodent tooth enamel. All but
539 one of the $\delta^{13}\text{C}$ ratios corresponds with a C_4 diet, indicating that both *Stegodon* and
540 murine rodents were predominantly grazers in both fossil-bearing horizons. The
541 positive shift observed in $\delta^{18}\text{O}$ of the younger *Stegodon* samples (from the hominin-
542 bearing Layer II) is more difficult to interpret with the limited data available, but
543 could mean a distinct source of drinking water (run-off versus lacustrine) and/or
544 warmer conditions; **b,** Benferroni corrected p values for a pairwise Mann-Whitney
545 statistical analysis to test for similarity of $\delta^{13}\text{C}$ between subsamples; **c,** Benferroni
546 corrected p values for a pairwise Mann-Whitney statistical analysis to test for
547 similarity of $\delta^{18}\text{O}$ between subsamples; p values showing significant differences in
548 median values are in bold.

549

550

551

552 **Extended Data Figure 9:** Analytical data for the Mata Menge stone technology. **a**,
553 Artefact counts and provenance, Trench E-32 (artefact definitions after ref. 37); **b**,
554 raw materials used to manufacture the stone tool assemblage, Trench E-32; **c**,
555 Platform types on flakes and modified flakes, E-32. Cortical: the blow was struck
556 onto the cortical surface of a cobble. Single-facet: the blow was struck on a scar
557 produced by previous reduction. Dihedral: the blow was struck on the ridge between
558 two scars produced by previous reduction. Multifacet: the blow was struck on the
559 surface of multiple small scars produced by previous reduction. Edge: the blow was
560 struck on the edge of the core and a platform surface is not retained on the flake; **d**,
561 Cortex coverage on the dorsal surface of complete unmodified flakes, E-32. Percent
562 cortex coverage refers to the proportion of the dorsal surface covered in cortex; **e**,
563 Artefact counts, Trenches E-32 and E-23/27 (artefact definitions after ref. 37); **f**, Sizes
564 of artefacts and attributes, E-32 and E-23/27; **g**, Raw materials used to manufacture
565 the stone tool assemblage, E-32 and E-23/27; **h**, Scatterplot of complete flake sizes,
566 E-32 (total sample size [N] = 68 complete flakes) and E-23/27 (N=443). With regards
567 to raw materials, coarse- and medium-grained materials include andesite, basalt,
568 rhyolite, and tuff. Fine-grained materials include silicified tuff, chalcedony, and opal.
569

570 31. Pearce, N. J. G. *et al.* A compilation of new and published major and trace element
571 data for NIST SRM 610 and NIST SRM 612 glass reference materials. *Geost. Newslet.*
572 **21**, 115-144 (1997).

573

- 574 32. Pearce, N. J. G. *et al.* Trace-element analysis by LA- ICP-MS: the quest for
575 comprehensive chemical characterisation of single sub-10µm volcanic glass shards.
576 *Quat. Int.* **246**, 57 - 81 (2011).
577
- 578 33. Deino, A. & Potts, R. Age-probability spectra for examination of single-crystal
579 $^{40}\text{Ar}/^{39}\text{Ar}$ dating results: Examples from Olorgesailie, southern Kenya Rift. *Quat. Int.*
580 **13–14**, 47–53 (1992).
581
- 582 34. Powell, R., Hergt, J. & Woodhead, J. Improving isochron calculations with robust
583 statistics and the bootstrap. *Chem. Geol.* **185**, 191–204 (2002).
584
- 585 35. Lee, J.-Y. *et al.* A redetermination of the isotopic abundances of atmospheric Ar.
586 *Geochim. Cosmochim. Acta* **70**, 4507–4512 (2006).
587
- 588 36. Duval, M. & Grün, R. Are published ESR dose assessments on fossil tooth enamel
589 reliable? *Quat. Geochron.* **31**, 19–27 (2016).
590
- 591 37. Moore, M.W. *et al.* 2009. Continuities in stone flaking technology at Liang Bua,
592 Flores, Indonesia. *J. Hum. Evol.* **57**, 503–526 (2009).
593
594
595
596
597
598

604 valley towards the northeast; **d**, stratigraphy and chronology of the main fossil-
605 bearing intervals and intervening Ola Bula Formation (OBF) deposits at Mata Menge.
606 Several basin-wide key marker tephra beds that are exposed in the hill flank on the
607 northern side of Mata Menge (trench E-34/34B) are eroded in the central part of the
608 stream valley, where they are replaced by a 4-5 m thick sequence of tuffaceous
609 mudflows with intervening fluvial lenses forming the lower fossil-bearing
610 paleovalley-fill sequence; **e-f**, context of the hominin fossils; **f** is a 3D image of Mata
611 Menge and surrounds, with excavated trenches outlined in red and labelled, and **e** is a
612 3D representation of the stratigraphy exposed by trench E-32A-E, with coloured ovals
613 denoting the positions of *in situ* hominin fossils (SOA-MM1, 2 and 4-6) excavated
614 from the fluvial sandstone unit, Layer II. Trenches E-1 to E-8 were excavated
615 between 2004-06, at the section originally excavated by Th. Verhoeven in the
616 1950s^{5,6}. The remaining trenches were excavated between 2010 to 2015. Tephra codes
617 in **d** are as follows (top to bottom): T6 (upper inter-regional tephra); PGT-2 (Piga
618 Tephra 2); T-UMM (Upper Mata Menge Tephra); T-LMM (Lower Mata Menge
619 Tephra); T-Pu (Pu Maso Tephra); T3 (lower inter-regional tephra); T-T (Turakeo
620 Tephra); T-WSI (Wolo Sege Ignimbrite); T-W (Wolowawu Tephra). The original
621 published $^{40}\text{Ar}/^{39}\text{Ar}$ age for T-WSI is 1.02 ± 0.02 Ma (ref. 13); however, when
622 recalculated to the recently determined value for the age standard ACS-2 used in this
623 study (1.185 Ma; see SI ref. 25), T-WSI becomes 1.01 ± 0.02 Ma.

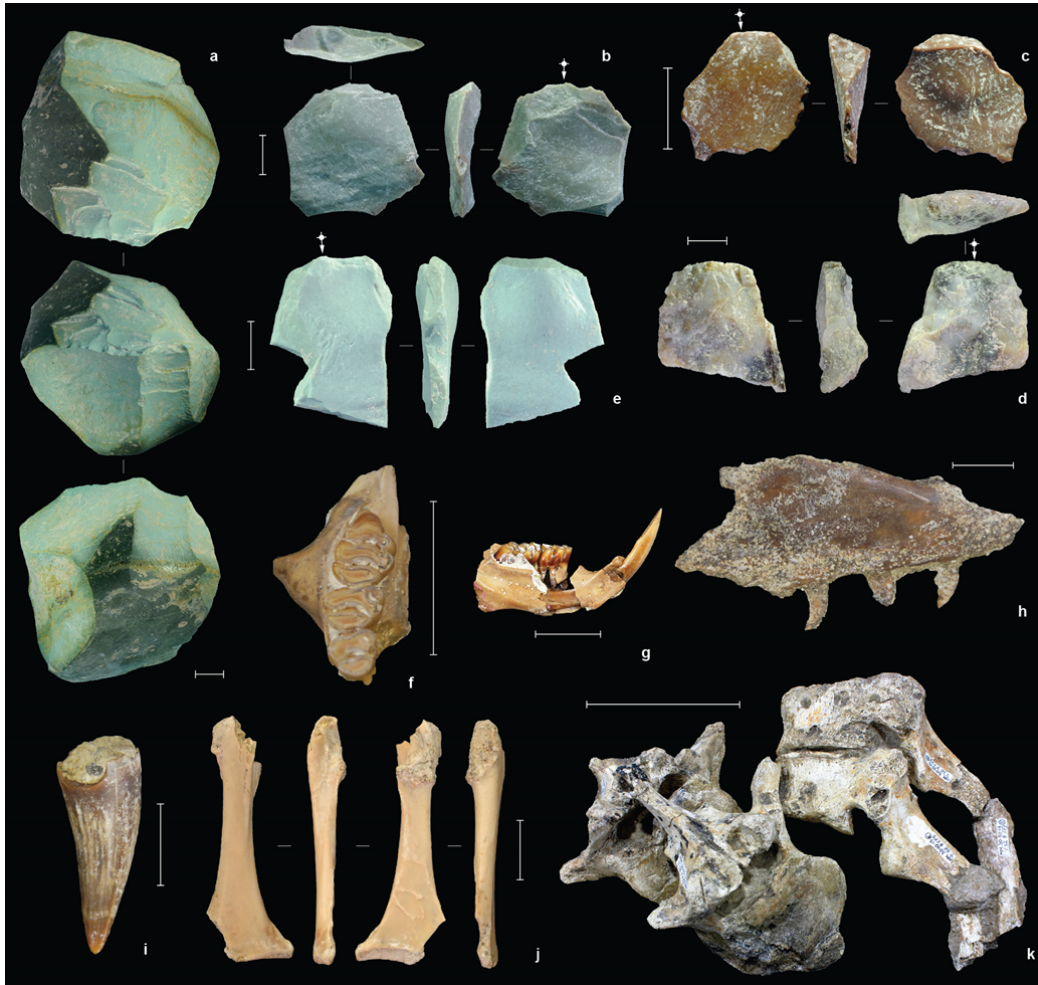
624

625

626

627

628



629

630 **Figure 2:** Stone artefacts and fossils from Mata Menge. All specimens are from the
631 hominin fossil find-locality (Layer II fluviatile sandstone, Trench E-32). **a**, bifacial
632 core (chlorite); **b-c**, chert flakes; **d**, chalcedony flake; **e**, rhyolite flake; **f**, right maxilla
633 fragment (M1-M3), *Hooijeromys nusatenggara*; **g**, left mandible fragment (m1-m3, i)
634 *H. nusatenggara*; **h**, right maxilla fragment, *Varanus komodoensis*; **i**, crocodile tooth;
635 **j**, right coracoid of a duck (cf. *Tadorna*); **k**, *Stegodon florensis* thoracic vertebrae in
636 articulation (still partially embedded in sandstone matrix). Scale bar lengths: **a-i** = 10
637 mm; **j** = 100 mm.

638

639

640



641

642

643 **Extended Data Figure 1. Hominin fossil find-locality at Mata Menge.** a, View of

644 Excavation 32 (trench E-32) in 2014, taken towards the north-north-west. The dip

645 slope visible in the background is the eastern flank of the Welas Caldera, which was
646 the source for many of the volcanic products deposited in the So'a Basin; **b**, E-32A-E
647 viewed towards the southwest, in October 2015; **c**, E-32D to E-32E viewed towards
648 the southwest. The irregular erosional upper surface of the reddish brown paleosol
649 (Layer III) formed the hardened bedding of a small stream. The sandy fossil-bearing
650 Layer II infills depressions formed on this bedding surface. A sequence of mudflows
651 (Layer I/a-f) rapidly covered the entire river bedding and its exposed banks; **d**, Mold
652 of a freshwater gastropod (Cerithoidea) from a sandy lens in Layer II; **e**, Detail of the
653 locally developed, gradual boundary between sandy Layers II and muddy Layer I.
654 Note the abundance of muddy rip clasts around the transition. At other places, the
655 boundary is sharp; **f**, West baulk of E-32C. Large *Stegodon florensis* bones occur at
656 the boundary between Layers II and I.

657

658

659

660

661

662

663

664

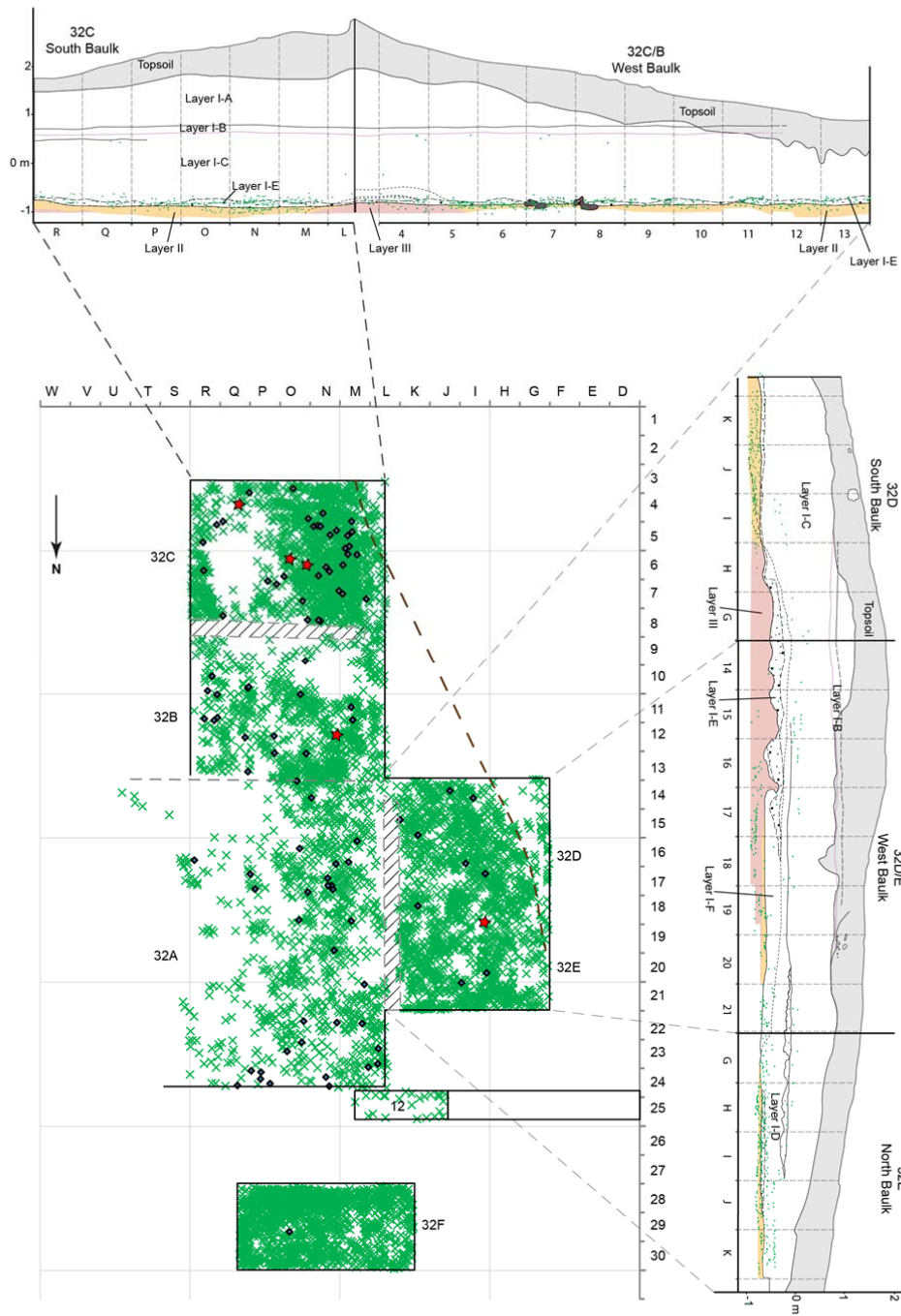
665

666

667

668

669



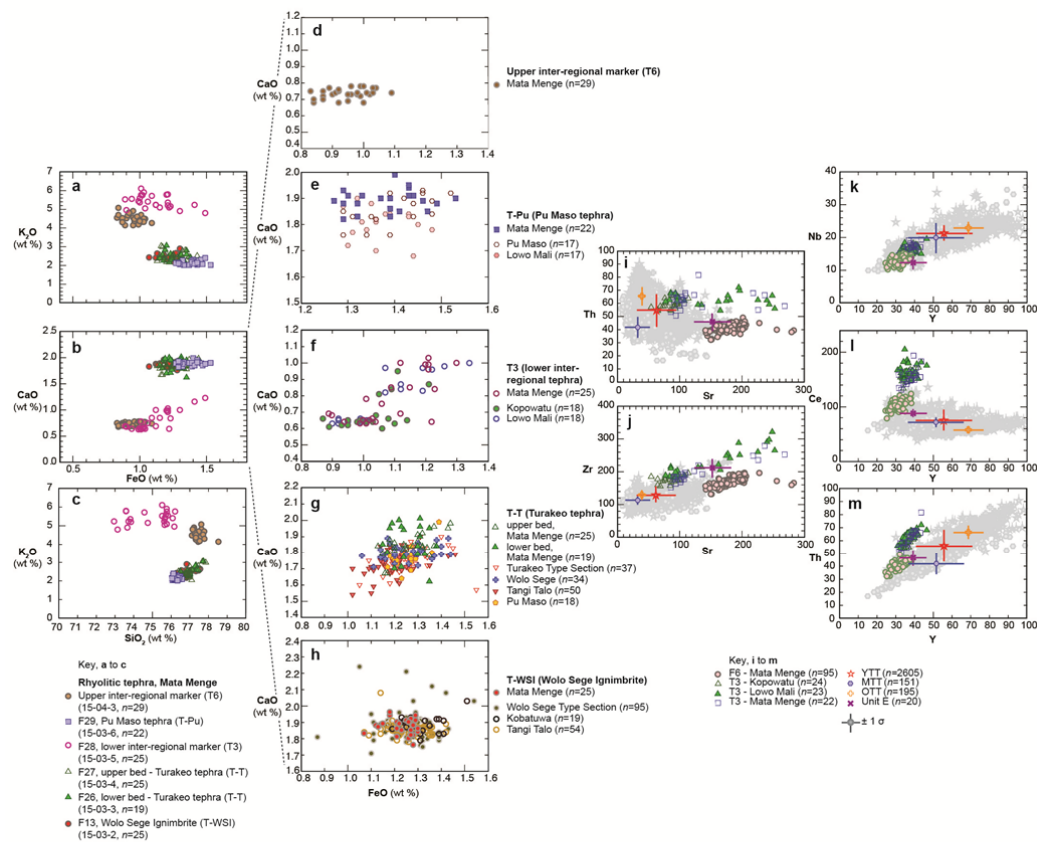
670

671 **Extended Data Figure 2: Plan and baulk profiles of Excavation 32A-F showing**

672 **distribution of finds.** The horizontal plan (lower left corner) shows the horizontal

673 coordinates of individual fossil finds (green crosses) and stone artefacts (blue

674 diamonds). The original position of hominin fossils is indicated with red stars. In the
675 trench baulk profiles (top and right) only the projected positions of fossil finds
676 occurring within one meter of the baulks are plotted. All hominin fossils were
677 recovered from the top of sandy Layer II. The basal part of the mudflow unit (Layers
678 Ia-e) also contains fossils, stone artefacts, gastropods, and pebbles. The thick brown
679 dotted line indicates the western margin of the ancient streambed.
680



681

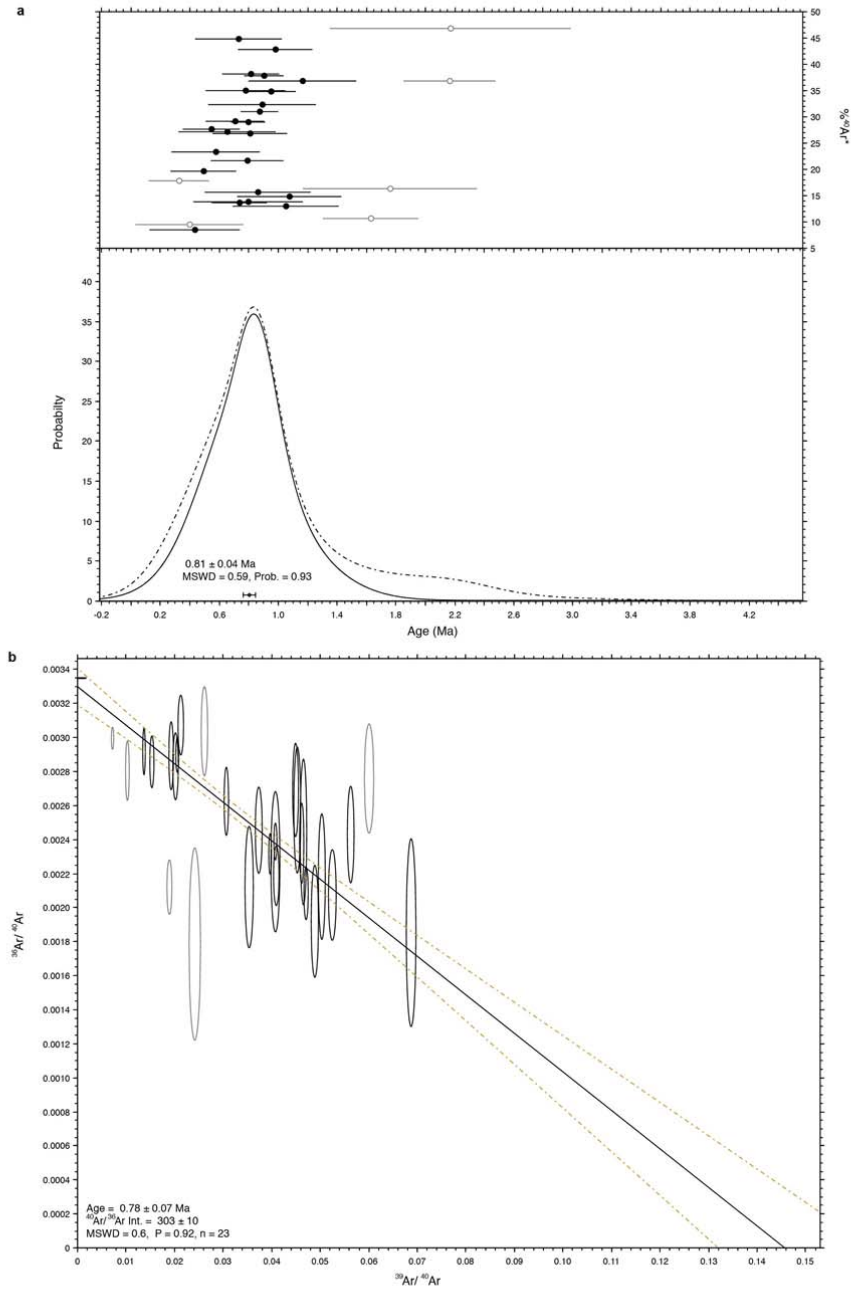
682 **Extended Data Figure 3: ITPFT dating and glass chemistry analysis. a-c,**

683 Selected major element compositions (weight percent FeO vs. K₂O and CaO and SiO₂

684 vs. K₂O) of glass shards from key rhyolitic pyroclastic density current (PDC) and

685 airfall deposits at Mata Menge; **d-h**, Weight percent FeO versus CaO composition of

686 glass shards from key rhyolitic pyroclastic density current (PDC) and airfall deposits
687 at Mata Menge (in stratigraphic sequence – youngest to oldest) compared with
688 correlatives from adjacent So'a Basin sites. While the major element glass
689 compositions of T-WSI, T-T and T-Pu are all geochemically indistinguishable (i.e.,
690 they are most likely from the same eruptive source) the major element data for each of
691 the tephra consistently occupies different overlapping fields. Moreover, while subtle
692 geochemical differences exist between T-WSI, T-T and T-Pu, these tephra can also be
693 readily distinguished in the field by a combination of stratigraphic position and
694 association, as well as by morphological expression; **i-j**, Selected trace element
695 compositions Sr versus Th and Zr, and **(k-m)** Y versus Nb, Ce and Th of glass shards
696 from T3 correlatives at Mata Menge, Lowo Mali and Kopowatu as well as T6
697 (uppermost inter-regional marker) from Mata Menge. All trace element
698 concentrations are in ppm unless otherwise stated. This data is plotted against
699 equivalent elemental mean and standard deviation (represented as $\pm 1\sigma$ error bars)
700 reference data from potential distal tephra correlatives (i.e. Youngest Toba Tuff
701 [YTT], Middle Toba Tuff [MTT], Oldest Toba Tuff [OTT] and Unit E from ODP-
702 758) acquired on the same instrument using the same standards and under the same
703 analytical conditions^{31,32}. Trace element data indicates that the upper (T6) and lower
704 (T3) inter-regional marker beds occurring at Mata Menge cannot be geochemically
705 related to any known Toba-sourced tephra. On this basis, the eruptive sources of T6
706 and T3 currently remain unknown. However, this absence of eruptive source certainly
707 does not diminish their importance within the overall So'a Basin stratigraphy.
708
709
710



711

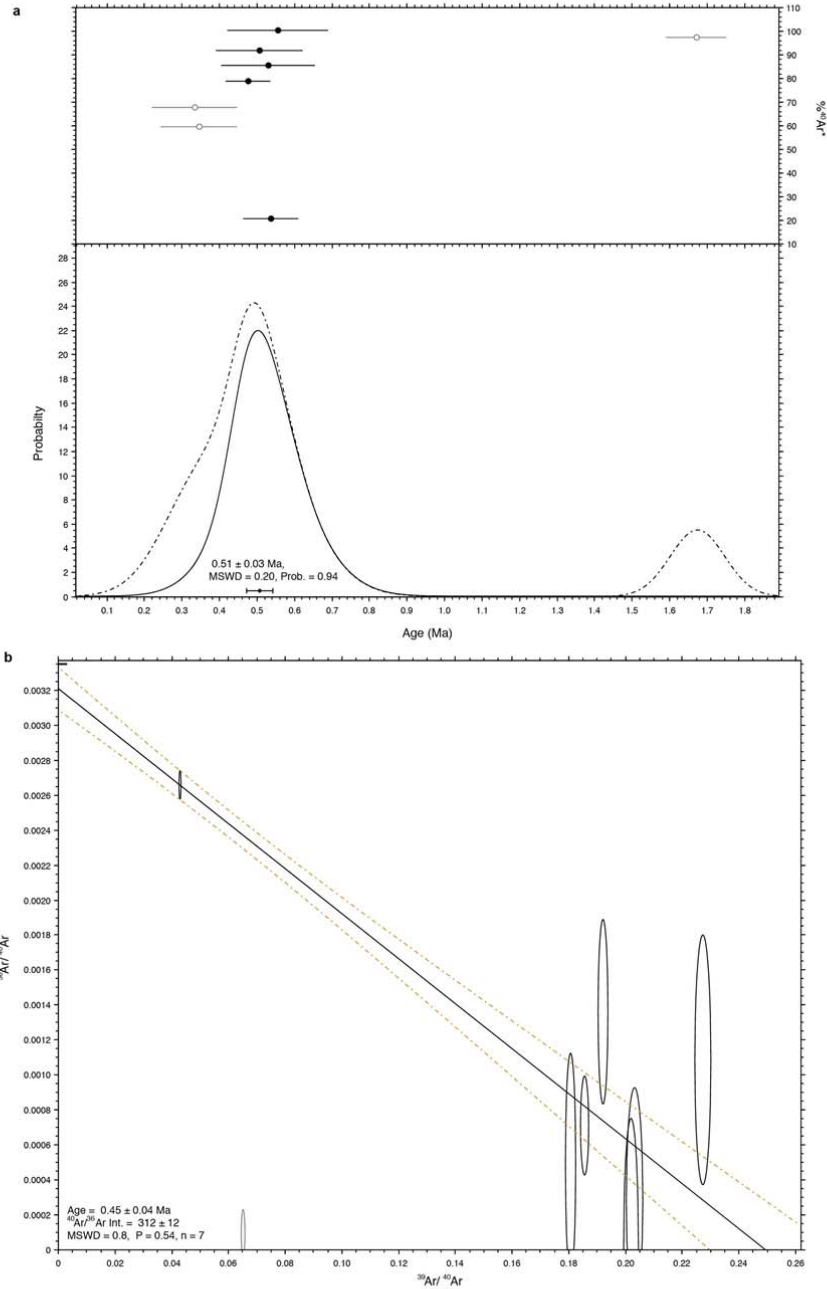
712 **Extended Data Figure 4: $^{40}\text{Ar}/^{39}\text{Ar}$ dating results.** **a**, Age probability plot for single

713 crystal laser fusion data for hornblende from the Pu Maso ignimbrite (sample FLO-

714 15-15; SI Table 5); the vertical scale is a relative probability measure of a given age

715 occurring in the sample³³. We applied an outlier-rejection scheme to the main
716 population to discard ages with normalized median absolute deviations of >1.5 (ref.
717 34) and these are shown as open circles. %⁴⁰Ar* refers to the proportion of
718 radiogenic ⁴⁰Ar released for individual analyses. The weighted mean age of the
719 filtered hornblende data for the Pu Maso ignimbrite is 0.81 ± 0.04 Ma ($1 \square \square \square$ mswd =
720 0.59, prob = 0.93; n = 23/29). An inverse isochron plot (**b**) for these 23 analyses gives
721 a statistically overlapping age of 0.78 ± 0.07 Ma (1σ ; mswd = 0.6, prob. = 0.92). The
722 ⁴⁰Ar/³⁶Ar intercept of 303 ± 10 is statistically indistinguishable from the atmospheric
723 ratio of 298.6 ± 0.3 (ref. 35), thus supporting the more precise weighted mean age
724 result.
725

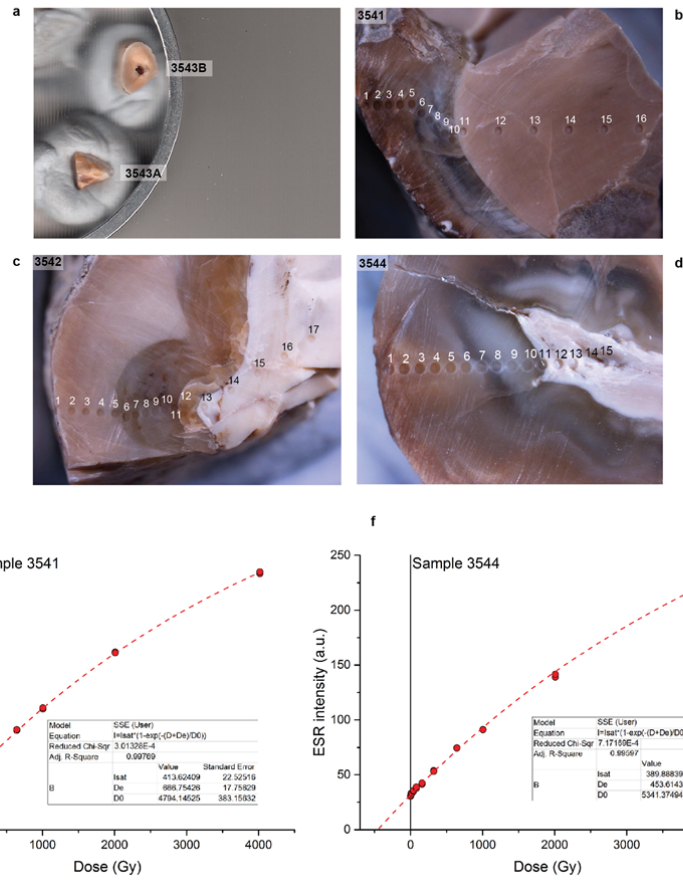
730 261; SI Table 5). $^{40}\text{Ar}^*$ ranges from < 10% to nearly 60%. The weighted mean age of
731 the filtered hornblende data for the PGT-2 tephra is 0.65 ± 0.02 Ma (1σ ; mswd = 0.78,
732 prob = 0.71; n = 17/24). An inverse isochron plot (**b**) gives a statistically overlapping,
733 but less precise age of 0.61 ± 0.04 Ma (1σ ; mswd = 1, prob. = 0.19).
734
735



736

737 **Extended Data Figure 6: $^{40}\text{Ar}/^{39}\text{Ar}$ dating results.** **a**, Age probability plot for single
 738 crystal laser fusion data for anorthoclase from the T6 upper inter-regional rhyolitic
 739 tephra (sample FLO15-09/2; SI Table 5). $^{40}\text{Ar}^*$ ranges from 20% to nearly 100%. The

740 weighted mean age of the filtered feldspar data for the T6 tephra is 0.51 ± 0.03 Ma
741 (1σ ; $\text{mswd} = 0.20$, $\text{prob} = 0.94$; $n = 5/8$). An inverse isochron plot (**b**) gives a
742 statistically overlapping, but less precise age of 0.45 ± 0.04 Ma (1σ ; $\text{mswd} = 0.8$,
743 $\text{prob.} = 0.54$).
744



745

746 **Extended Data Figure 7: U-series and ESR samples and dating results. a,**

747 Hominin tooth root samples (#3543A and #3543B) from Layer II, Mata Menge; **b, d,**

748 U-series laser tracks for *Stegodon* molar samples from Layer II; **e, f**, Dose response

749 curves obtained for the two powder enamel samples from #3541 and #3544,
750 respectively. Fitting was carried out with a SSE function through the pooled mean
751 ESR intensities derived from each repeated measurement. Given the magnitude of the
752 D_E values, the correct D_E value was obtained for $5 > D_{\max}/D_E > 10$ (ref. 36).

753

754

755

756

757

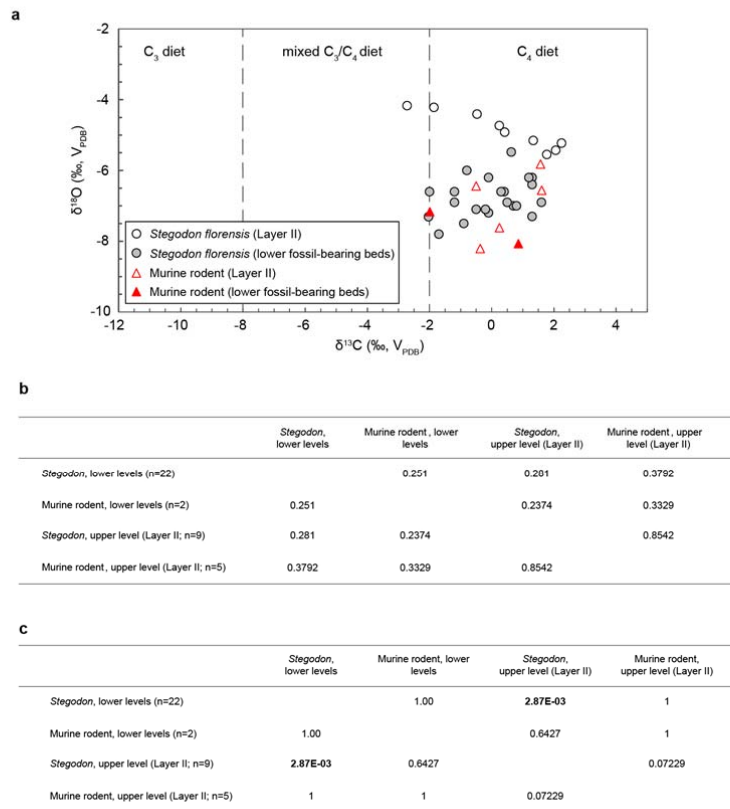
758

759

760

761

762



763

764 **Extended Data Figure 8. Carbon and oxygen isotope analysis of dental enamel. a,**

765 $\delta^{13}\text{C}$ and $\delta^{18}\text{O}$ values of *Stegodon florensis* and murine rodent tooth enamel. All but

766 one of the $\delta^{13}\text{C}$ ratios corresponds with a C_4 diet, indicating that both *Stegodon* and

767 murine rodents were predominantly grazers in both fossil-bearing horizons. The

768 positive shift observed in $\delta^{18}\text{O}$ of the younger *Stegodon* samples (from the hominin-

769 bearing Layer II) is more difficult to interpret with the limited data available, but

770 could mean a distinct source of drinking water (run-off versus lacustrine) and/or

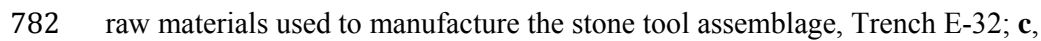
771 warmer conditions; **b**, Benferroni corrected p values for a pairwise Mann-Whitney

772 statistical analysis to test for similarity of $\delta^{13}\text{C}$ between subsamples; **c**, Benferroni
773 corrected p values for a pairwise Mann-Whitney statistical analysis to test for
774 similarity of $\delta^{18}\text{O}$ between subsamples; p values showing significant differences in
775 median values are in bold.

776

777

778



783 Platform types on flakes and modified flakes, E-32. Cortical: the blow was struck
784 onto the cortical surface of a cobble. Single-facet: the blow was struck on a scar
785 produced by previous reduction. Dihedral: the blow was struck on the ridge between
786 two scars produced by previous reduction. Multifacet: the blow was struck on the
787 surface of multiple small scars produced by previous reduction. Edge: the blow was
788 struck on the edge of the core and a platform surface is not retained on the flake; **d**,
789 Cortex coverage on the dorsal surface of complete unmodified flakes, E-32. Percent
790 cortex coverage refers to the proportion of the dorsal surface covered in cortex; **e**,
791 Artefact counts, Trenches E-32 and E-23/27 (artefact definitions after ref. 37); **f**, Sizes
792 of artefacts and attributes, E-32 and E-23/27; **g**, Raw materials used to manufacture
793 the stone tool assemblage, E-32 and E-23/27; **h**, Scatterplot of complete flake sizes,
794 E-32 (total sample size [N] = 68 complete flakes) and E-23/27 (N=443). With regards
795 to raw materials, coarse- and medium-grained materials include andesite, basalt,
796 rhyolite, and tuff. Fine-grained materials include silicified tuff, chalcedony, and opal.
797
798
799

